Determination of gold nanoparticle shape from absorption spectroscopy and ellipsometry

Yann Battie, Irene Izquierdo-Lorenzo, Amandine Resano-Garcia, Aotmane En Naciri, Suzanna Akil, Pierre-Michel Adam, Safi Jradi

Determination of gold nanoparticle shape from absorption spectroscopy and ellipsometry

Yann Battie, Irene Izquierdo-Lorenzo, Amandine Resano-Garcia, Aotmane En Naciri, Suzanna Akil, Pierre-Michel Adam, Safi Jradi

Full Length Article

Determination of gold nanoparticle shape from absorption spectroscopy and ellipsometry

Yann Battie [a,*], Irene Izquierdo-Lorenzo [b], Amandine Resano-Garcia [a], Aotmane En Naciri [a], Suzanna Akil [b], Pierre Michel Adam [b], Safi Jradi [b]

[a] LCP-A2MC, Institut Jean Barriol, Université de Lorraine, 1 Bd Arago, 57070 Metz, France
[b] LNIO (CNRS UMR 6279), Université de Technologie de Troyes, 12 rue Marie Curie, 10010 Troyes, France

ARTICLE INFO

Article history:
Received 28 July 2016
Received in revised form
21 November 2016
Accepted 19 December 2016
Available online xxx

Keywords:
Ellipsometry
Absorption spectroscopy
Nanoparticle shape distribution
Effective medium theory

ABSTRACT

A new methodology is developed to determine the shape distribution of gold nanoparticles (NPs) from optical spectroscopic measurements. Indeed, the morphology of Au colloids is deduced by fitting their absorption spectra with an effective medium theory which takes into account the nanoparticle shape distribution. The same procedure is applied to ellipsometric measurements recorded on photoresist films which contain Au NPs. Three spaces (L^2, r^2, P^2) are introduced to interpret the NPs shape distribution. In the P^2 space, the sphericity, the prolacity and the oblacity estimators are proposed to quantify the shape of NPs. The r^2 space enables the determination of the NP aspect ratio distribution. The distributions determined from optical spectroscopy were found to be in very good agreement with the shape distributions obtained by transmission electron microscopy. We found that fitting absorption or ellipsometric spectra with an adequate effective medium theory, provides a robust tool for measuring the shape and concentration of metallic NPs.

1. Introduction

Metallic nanoparticles (NPs) such as silver or gold NPs exhibit strong plasmon resonances whose characteristics depend on their size, shape and environment [1]. These unique optical properties give them great potentials as building blocks of photovoltaic devices and sensors [2–6]. These applications have motivated a sustained effort towards the control of NP size and shape distributions. Transmission electron microscopy (TEM) is usually used to estimate the NP radius and shape distribution. However, since TEM is a local characterization tool, the statistical analysis of NP distributions from TEM is too time consuming. In addition, TEM only gives a two dimensional projection of NPs. This could lead to a poor estimation of NP shape. Tomography mode is currently under development and is not implemented on conventional TEM. Moreover, the 3D observation of NPs in tomography mode is too time consuming to record their distribution over a huge number of NPs. Thus, the development of non-local alternative characterization tools is required to determine the NP shape distribution. Grazing incidence small angle X-ray scattering (GISAXS) was previously used to characterized the morphology of supported NPs [7–9]. The shape distribution can be estimated by comparing the measured GISAXS pattern with the simulated one. However, this technique requires some facilities such as synchrotron beam line. In addition, this technique cannot be used to characterize NPs in bulk solution or embedded in thick film.

Recent advances in optical modeling open new ways for quantitative optical characterization of metallic NPs. Garellie et al. [10] have introduced the NP size distribution into the Mie theory. However, Mie theory fails to describe the optical properties of non-spherical NPs [11]. As shown by Eustis et al. [12], the aspect ratio distribution of gold nanorods can be evaluated by fitting their longitudinal plasmon band by the Gans theory. Slyusarenko et al. [13] have validated this approach by comparing the NP volume fraction obtained from absorption spectroscopy to the one estimated by small angle X-Ray scattering measurement. However, Eustis et al. [12] neglect the influence of the aspect ratio distribution on the interband transitions and on the transversal plasmon band of NPs. In addition, this approach is limited to prolate NPs. Spectroscopic ellipsometry has been recently exploited to investigate the growth mechanism of metallic NPs [14–17]. As shown by Oates et al. [15,16], the NP size, orientation and organization can be characterized by spectroscopic ellipsometry. The analysis of ellipsometric data requires the modeling of the optical properties of nanomate-

* Corresponding author.
E-mail address: yann.battie@univ-lorraine.fr (Y. Battie).

Please cite this article in press as: Y. Battie, et al., Determination of gold nanoparticle shape from absorption spectroscopy and ellipsometry, Appl. Surf. Sci. (2016), http://dx.doi.org/10.1016/j.apsusc.2016.12.167

rials. Several approaches such as discrete dipole approximation [18] or boundary elements method [19] can be used to model the optical properties of complex NP shapes. However, these approaches are limited by computational resources and are too time consuming to take into account the NP shape distribution.

Effective medium theories which approximate the nanocomposite material as a homogeneous medium, enable the calculation of its effective dielectric function with few computational resources. Toudert et al. [20] have proposed an effective medium theory based on the Yamaguchi formalism which takes into account the NP interaction and their size distribution. However, this model requires a preliminary estimation of the pair correlation function of NPs by transmission electron microscopy. Another approach based on the mean field approximation was proposed by Bohren et al. [21] to extend the effective medium theory to ellipsoidal nanoparticles distributed in shape. This shape distributed effective medium theory (SDEMT) was used to design broadband epsilon-near zero composites [22] and to analyze ellipsometric measurements on gold nanoisland films [23] or absorption measurements on gold colloids [24–26]. However, the NP shape distribution is represented in a complex two dimensional space of depolarization parameters making the interpretation of the NP shape unclear.

In this paper, we determine the NP shape distribution of two gold colloidal solutions and two photoresist films which contain gold nanoparticles by fitting their absorption and ellipsometric spectra with the SDEMT, respectively. To make a quantitative analysis, we introduce two new spaces P^2 and r^2 derived from the space of depolarization parameter L^2 to interpret the shape distribution of NPs. The coordinates (P_o, P_p) in the P^2 space are assimilated as estimators of the oblate and prolate character of NPs, respectively. In addition, the coordinates (r_1, r_2) in the r^2 space correspond to the aspect ratio of ellipsoïdal NPs. Thus, by using SDEMT combined to an adequate space transformation, we demonstrate that the nanoparticle shape distribution can be directly extracted from optical spectroscopy.

2. Theory

2.1. Shape distributed effective medium theory (SDEMT)

The effective dielectric function ε_{eff} of a medium composed of ellipsoidal NPs distributed in shape and randomly oriented in a matrix is defined as the ratio between the spatial averages of displacement <**D**> and electric <**E**> fields:

$$\varepsilon_{\text{eff}} = <\mathrm{D}><\mathrm{E}>^{-1}. \tag{1}$$

In the mean field approximation, the spatial averages of electric <**E**> and displacement <**D**> fields in the material are the sum of two contributions [21]:

$$\langle \mathbf{E} \rangle = (1-f)\langle \mathbf{E_m} \rangle + f\langle \mathbf{E_{np}} \rangle, \tag{2}$$

$$\langle \mathbf{D} \rangle = (1-f)\varepsilon_m \langle \mathbf{E_m} \rangle + f\varepsilon_{np}\langle \mathbf{E_{np}} \rangle, \tag{3}$$

where ε_{np} and ε_m are the complex dielectric function of NPs and the matrix, respectively. f is the NP volume fraction of NPs while <$\mathbf{E}_m$> and <$\mathbf{E}_{np}$> are the spatial average electric field inside the matrix and NPs, respectively.

In the quasi-static limit i.e. for NP size smaller than the wavelength, we derive a linear relationship between the electric field inside NPs and the electric field inside de matrix. For small NP volume fraction, the electric field inside the matrix is homogeneous and the spatial average electric field inside the NPs is related to the spatial average electric field inside the matrix by:

$$\langle \mathbf{E_{np}} \rangle = \langle \beta \rangle \langle \mathbf{E_m} \rangle. \tag{4}$$

The slope <β > is given by [26]:

$$\langle \beta \rangle = \frac{\varepsilon_m}{3} \int\int P(L_1, L_2) \sum_{i=1}^{3} \frac{1}{\varepsilon_m + L_i\left(\varepsilon_{np}(l) - \varepsilon_m\right)} dL_1 dL_2. \tag{5}$$

L_1, L_2, L_3 are the depolarization parameters of ellipsoïdal NPs along their three principal axis. These parameters which depend on the NP shape, vary in the 0–1 range and must respect the following sum rule:

$$1 = L_1 + L_2 + L_3 \tag{6}$$

Note that this equation fails for NPs located on an interface. In this case, dipole images must be taken into account. Other theories such as the Yamaguchi theory [27] or the Bedeaux and Viegler theory [28,29] must be considered to take into account dipole image effects. The distribution of the depolarization parameters ($P(L_1, L_2)$) is introduced into Eq. (5) to take into account the distribution of NP shape. The effective dielectric function of a medium composed of ellipsoidal NPs embedded in a dielectric matrix can be calculated by combining Eqs. (1)–(4):

$$\varepsilon_{eff} = \frac{(1-f)\varepsilon_m + f\varepsilon_{np}\langle\beta\rangle}{(1-f) + f\langle\beta\rangle}. \tag{7}$$

This effective dielectric function respects the Wiener limits and Hashin-Shtrikman bounds. In the following, we assume that the distribution of depolarization parameters is described by a sum of Gaussian distributions [24,26]:

$$P(L_1, L_2) = C\sum_{k=1}^{N} C_k e^{-0.5\left(\frac{(L_1-\bar{L}_{1k})^2}{\sigma_{1k}^2} + \frac{(L_2-\bar{L}_{2k})^2}{\sigma_{2k}^2} + \frac{(L_3-\bar{L}_{3k})^2}{\sigma_{3k}^2}\right)}. \tag{8}$$

Note that other distributions can be used. C is a constant used to normalize the distribution. $\sigma_{i,k}$ and $\bar{L}_{i,k}$ are the standard deviation and the mean value of L_i of the k^{th} Gaussian term, respectively. $\bar{L}_{1,k}$, $\bar{L}_{2,k}$ and $\bar{L}_{3,k}$ are linked together by Eq. (6). The relative volume fraction f_k attributed to the k^{th} Gaussian term is defined by:

$$f_k = fCC_k. \tag{9}$$

2.2 L^2, P^2 and r^2 spaces

By considering the Bohren convention [21] ($L_1 \le L_2 \le L_3$), we can define a two dimensional depolarization space (L^2) in which each NP shape is represented by an unique point $M(L_1, L_2)$ (Fig. 1a). In this space, the normalized distribution of NP depolarization factors $P(L_1, L_2)$ is correlated to the NPs shape distribution. As an example, the locus of spherical, oblate and prolate NPs are $L_1 = L_2 = 1/3$, $L_1 = L_2$ and $L_2 = 0.5–0.5L_1$, respectively. However, the quantitative description of nanoparticle shape distribution and the numerical calculation of the integral of Eq. (5) remain difficult in this physical space. As shown in Fig. 1a, each point M of the L^2 space is included in a ABC triangle. Thus, the vector **AM** must respect the following relationship:

$$\boldsymbol{AM} = \left(1-P_p\right)\boldsymbol{AB} + (1-P_o)\left(1-P_p\right)\boldsymbol{BC}. \tag{10}$$

Where $0 \le P_o \le 1$ and $0 \le P_p \le 1$. Each point $M(L_1, L_2)$ can be represented by a new set of coordinates (P_0, P_p) in a two dimensional orthonormal space (P^2) (Fig. 1b). The (L_1, L_2) coordinates are related to the (P_1, P_2) coordinates thanks to the following transformations:

$$L_1 = \frac{(1-P_o)\left(1-P_p\right)}{3}. \tag{11}$$

$$L_2 = \frac{\left(1-P_p\right)}{2} - \frac{(1-P_o)\left(1-P_p\right)}{6} \tag{12}$$

The locus of oblate, prolate or spherical NPs in P^2 are $(0, P_p)$, $(P_o, 0)$ and $(0, 0)$, respectively. In other words, P_o and P_p traduce

Please cite this article in press as: Y. Battie, et al., Determination of gold nanoparticle shape from absorption spectroscopy and ellipsometry, Appl. Surf. Sci. (2016), http://dx.doi.org/10.1016/j.apsusc.2016.12.167

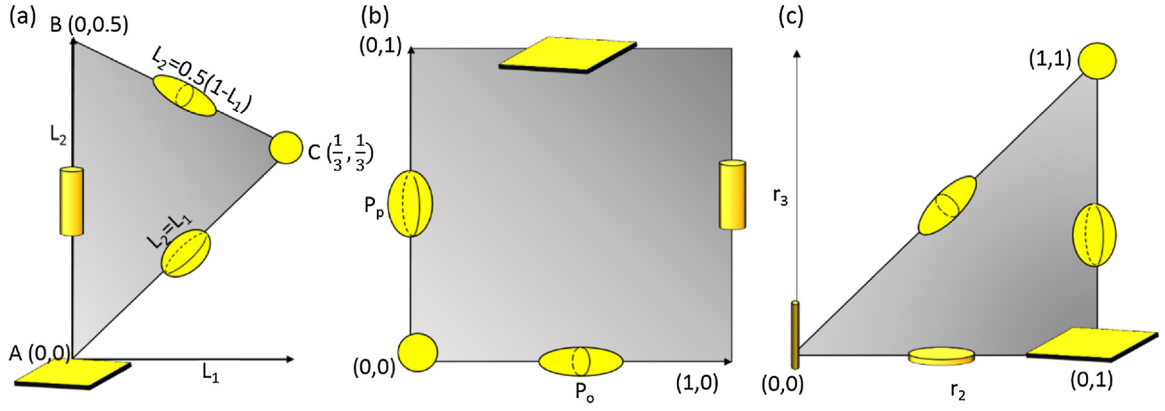

Fig. 1. Schematic representation of (a) L^2, (b) P^2 and (c) r^2 spaces. The locus of spherical, prolate, oblate, cylinder NPs are reported in all spaces.

the oblate and prolate characters of NPs, respectively. Indeed, the closer $P_0(P_p)$ value is to 0, the more nanoparticles can be considered as oblate (prolate).

To give a quantitative analysis of the NPs shape distribution in the P^2 space, we introduce three estimators: the oblacity ($\bar{P}_o$), the prolacity ($\bar{P}_p$) and the sphericity ($\bar{P}_s$) of NPs. ($\bar{P}_o$, $\bar{P}_p$) are calculated by applying the coordinates transformation (11)–(12) to the mean value ($\bar{L}_1$, $\bar{L}_2$) of the depolarization parameter distribution. $\bar{P}_o$ and $\bar{P}_p$ quantifies the deviation of NPs to the oblate and prolate shapes respectively. Both estimators vary in the 0–1 range. The sphericity ($\bar{P}_s$) is the euclidian distance in the P^2 space between the locus of spherical NPs and the mean value of the distribution of NP shape:

$$\bar{P}_s = \sqrt{\bar{P}_o^2 + \bar{P}_p^2}. \tag{13}$$

This estimator which varies in the $0-\sqrt{2}$ range, enables an estimation of the deviation of NPs shape distribution from the spherical distribution. Indeed, the closer its value is to 0, the more the distribution can be considered as that of spherical distribution. Eq. (13) supports that spherical NPs have simultaneously a prolate and an oblate shape. Thus, the introduction of the P^2 space makes easier the quantitative analysis of the NP shape distribution.

By assuming that the effective medium is composed of ellipsoidal NPs, the distribution of depolarization factor $P(L_1,L_2)$ in the L^2 space can be converted into a distribution $P(r_2,r_3)$ in aspect ratios of ellipsoidal NPs in a new 2-dimensional space r^2 (Fig. 1c) by applying the following coordinate transformation [21]:

$$L_i = \frac{r_2 r_3}{2} \int_0^{+\infty} \frac{dq}{\left(q + r_i^2\right) \sqrt{\prod_{i=1}^{3} \left(q + r_i^2\right)}}, \tag{14}$$

where $r_i = a_i/a_1$ (i = 1–3) the aspect ratios of an ellipsoidal NP. a_1, a_2, a_3 are the length of principal axes of each ellipsoidal NP. To obtain a bijective space, the lengths of principal axes are sorted in the following order: $a_3 \leq a_2 \leq a_1$.

3. Materials and methods

In this paper, two colloidal solutions of gold NPs (S1, S2) and two photoresists films (F1, F2) which contain gold NPs are considered.

The colloidal solution S1 of Au dispersed in water was purchased from Sigma Aldrich and was used as received. S2 was synthesized according to the seed-mediated growth method [30]. Briefly, a seed solution was prepared by mixing 5 ml of $HAuCl_4$ (5×10^{-4} M) dispersed in water with 5 ml of CTAB (0.2 M) and 0.6 ml of ice-cold $NaBH_4$ (0.01 M) solutions. Then, 12 μl of the seed solution was mixed to 5 ml of a CTAB (0.2 M), 0.3 ml of $AgNO_3$ (4×10^{-3} M), 5 ml of $HAuCl_4$ (0.001 M) and 70 μl of ascorbic acid (0.08 M).

F1 and F2 films are elaborated by the following procedure [31]: 5%/wt and 60%/wt of $HAuCl_4 \cdot 3H_2O$ were dispersed in propyleneglycol monomethyl ether acetate (PGMEA) for F1 and F2, respectively. These solutions were added to a commercial photoresists AZ9260. The proportion of PGMEA in AZ9260 is set at 70:30. The mixtures were homogenized in an ultrasonic bath for one minute at room temperature. The films are deposited on a cleaned silicon substrate by spin coating at 5000 rpm for 60 s. The films are baked on hot plate 8 min at 80 °C and 2 min at 120 °C to evaporate all traces of solvent and activate the growth of NPs. The F1 and F2 film thicknesses are 258 ± 1 nm and 105 ± 1 nm, respectively. The nominal volume fractions of NPs calculated from the amount of all reactants are 0.6% ± 0.1% and 12% ± 2% for F1 and F2, respectively.

Ellipsometric measurements were recorded in reflection mode in the 0.59–4.43 eV spectral range with a phase modulated ellipsometer (UVISEL, Horiba). The light beam diameter is approximately equal to 5 mm. The ellipsometric parameters *Is*, *Ic* were measured at three angles of incidence: 50°, 60° and 70°. These parameters depend on the ellipsometric angles Ψ and Δ:

$$I_s = sin2\Psi sin\Delta \tag{15}$$

$$I_c = sin2\Psi cos\Delta \tag{16}$$

Absorption spectroscopy was performed on S1 and S2 solution by using the same set up in transmission configuration. The solution is placed inside a quartz cuvette of 1 mm light path.

TEM images are recorded with a Technai CM200 microscope operating at 200 kV. TEM grids of S1 and S2 were prepared by evaporating a drop of colloidal solution on a copper grid. To prepare TEM grids of F1 and F2, the films are stripped off the substrate by scratching the samples with a razor blade. The film fragments are then deposited on a copper TEM grid.

4. Results and discussion

Fig. 2 shows the TEM images of S1, S2, F1 and F2 Au NPs. The length distributions of the apparent minor (d) and major axes (D) of NPs are reported in Fig. 3. S1 and F1 contain spherical Au nanoparticles whose mean diameters are 31 ± 3.6 nm and 6–7 ± 2 nm, respectively. S2 is composed of a mixture of spherical Au NPs and Au nanorods with a major axis length smaller than 45 nm. F2 is composed of NPs polydispersed in shape. Their mean diameter is estimated at 12–13 ± 6.8 nm. In agreement with the quasi-static approximation, the NP size deduced from TEM measurements is much smaller than the wavelength. In other words, scattering, multipolar and dynamic effects are negligible for this NP size [25].

Please cite this article in press as: Y. Battie, et al., Determination of gold nanoparticle shape from absorption spectroscopy and ellipsometry, Appl. Surf. Sci. (2016), http://dx.doi.org/10.1016/j.apsusc.2016.12.167

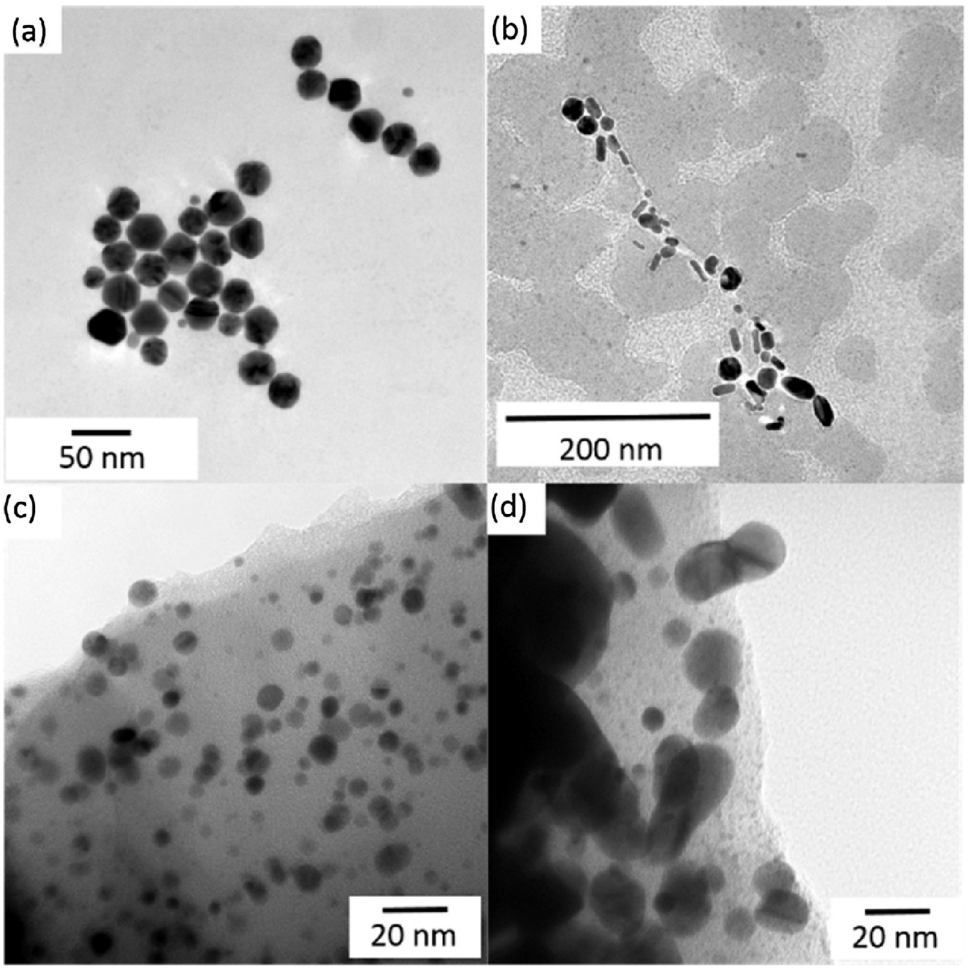

Fig. 2. TEM images of (a) S1, (b) S2, (c) F1 and (d) F2.

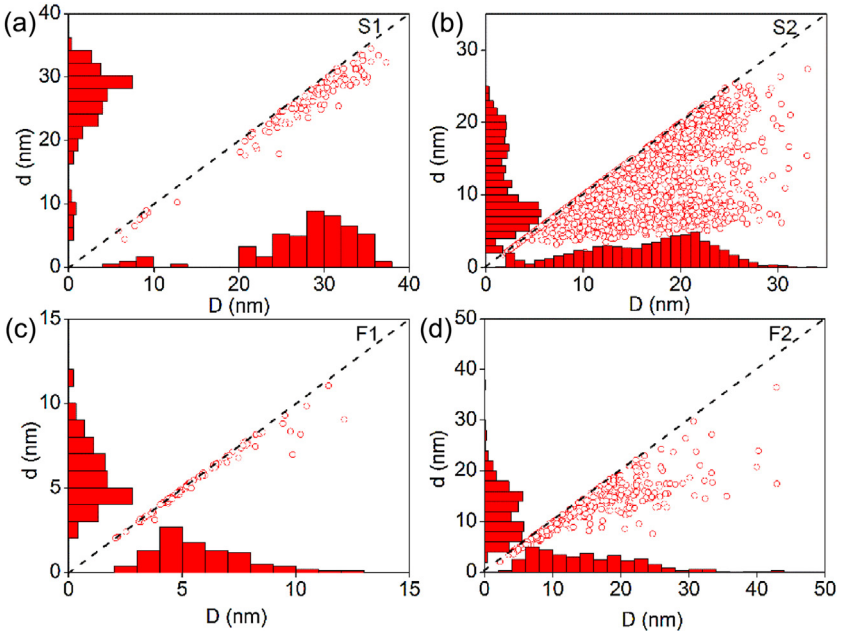

Fig. 3. Distributions of the lengths of the minor (d) and major (D) axes of (a) S1, (b) S2, (c) F1 and (d) F2 NPs.

Please cite this article in press as: Y. Battie, et al., Determination of gold nanoparticle shape from absorption spectroscopy and ellipsometry, Appl. Surf. Sci. (2016), http://dx.doi.org/10.1016/j.apsusc.2016.12.167

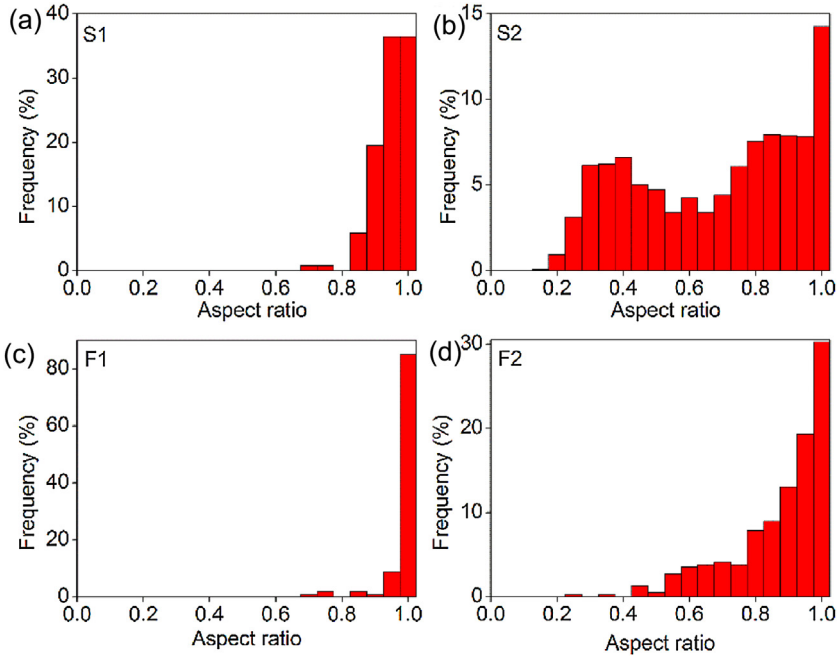

Fig. 4. Apparent aspect ratio distributions of (a) S1, (b) S2, (c) F1 and (d) F2 NPs.

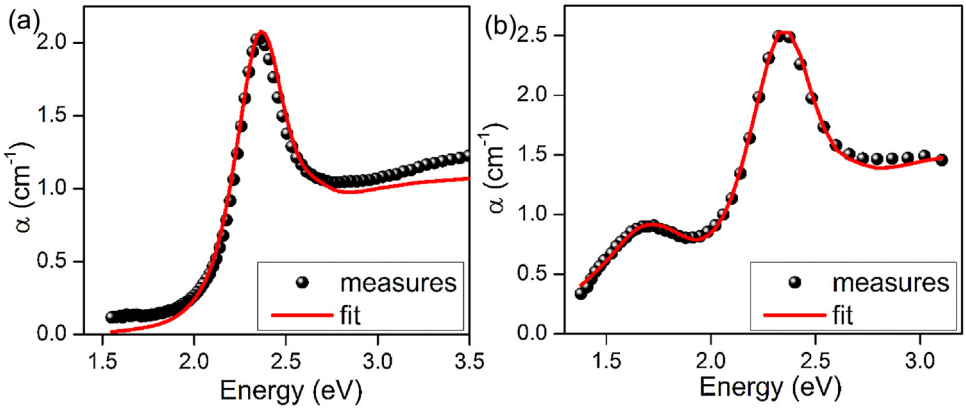

Fig. 5. Comparison between the measured and calculated absorption spectra of (a) S1 and (b) S2.

The NPs aspect ratio distributions measured from TEM are reported in Fig. 4. The aspect ratio of S1 NPs, defined as the ratio between the lower and the higher NP radius, is in the 0.8–1 range, confirming that S1 is mainly composed of spherical NPs. On the other hand, 86% of F1 NPs have an aspect ratio in the 0.95–1 range. In other words, F1 NPs are nearly monodispersed in shape. The aspect ratio distribution of S2 measured over 1500 NPs follows a bimodal distribution centered at 1 and 0.35 associated to nearly spherical NPs and nanorods, respectively. F2 is composed of randomly oriented nanoparticles which have a broad shape distribution. The amount of spherical NPs is estimated at 30% in F2 film. Indeed, most of NPs are elongated. These NPs come from the coalescence of spherical NPs.

The absorption spectra of S1 and S2 are shown in Fig. 5. The absorption due to the interband transitions of Au NPs is clearly observed above 2.5 eV. The absorption spectra of S1 exhibits a strong plasmon resonance located at 2.35 eV. The S2 spectra exhibits two overlapped broad bands centered at 1.677 eV and 2.34 eV. The band located at lower energy has a smaller amplitude than the band at higher energy. By considering the Fröhlich condition [1], which corresponds to the pole of Eq. (5), the bands at 2.35–2.36 eV can be assimilated to the optical signature of nearly spherical NPs while the band centered at 1.677 eV corresponds to the longitudinal plasmon resonance of Au nanorods. To analyze the NP shape distribution, the measured absorption spectra were fitted by using the SDEMT model. The dielectric function of NPs (ε_{np}) is assimilated to the dielectric function of bulk Au [32]. The dielectric function of the matrix (ε_m) is replaced by the dielectric function of water [32]. The Levenberg-Marquardt algorithm [33] is used to solve the inverse problem. By considering TEM measurements (Figs. 2 and 4), we assume that the distribution of depolarization parameters is described by a single Gaussian distribution for S1, and a sum of two Gaussian distributions for S2. Thus, 6 (f, $\bar{L}_1$, $\bar{L}_2$, σ_1, σ_2, σ_3) and 12 (f_1, $\bar{L}_{11}$, $\bar{L}_{21}$, σ_{11}, σ_{21}, σ_{31}, f_2, $\bar{L}_{12}$, $\bar{L}_{22}$, σ_{12}, σ_{22}, σ_{32}) free parameters are simultaneously fitted for S1 and S2, respectively. The correlation coefficients between free parameters are in the −0.6; 0.6 range, confirming that all parameters are not correlated. This behavior comes from the high sensitivity of each parameter to a specific characteristic of the spectra. Indeed, as we have demonstrated previously [26], the shape distribution has a negligible influence on the effective absorption coefficient in the UV spectral range. In this spectral range, a linear relationship can

Please cite this article in press as: Y. Battie, et al., Determination of gold nanoparticle shape from absorption spectroscopy and ellipsometry, Appl. Surf. Sci. (2016), http://dx.doi.org/10.1016/j.apsusc.2016.12.167

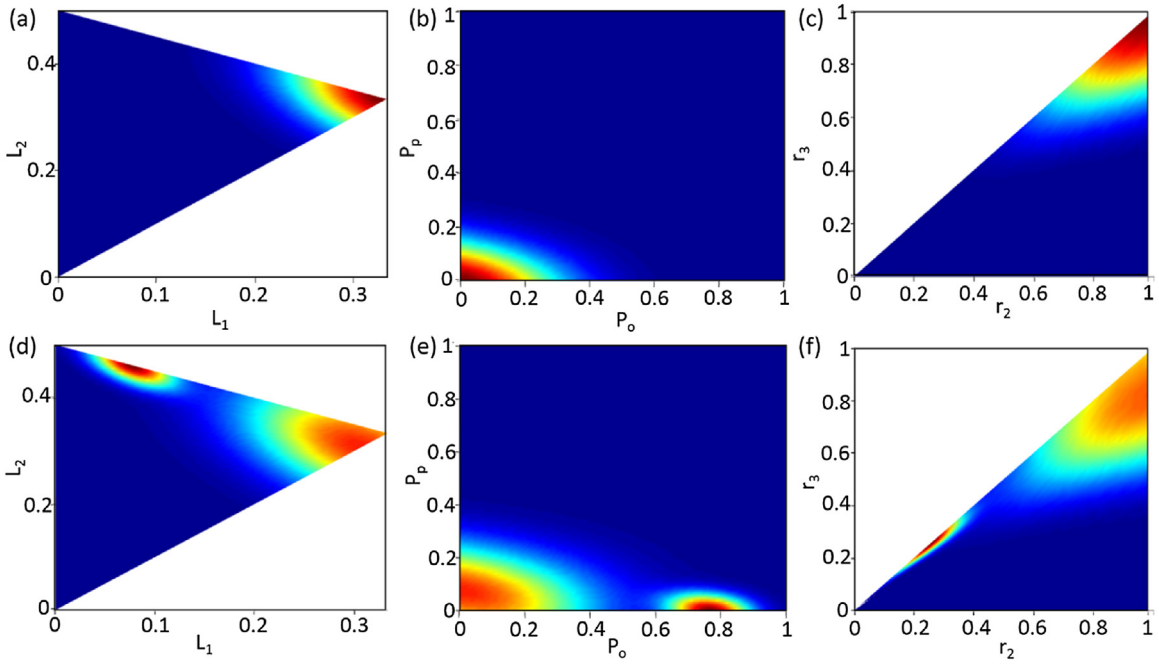

Fig. 6. Distributions of (a)–(c) S1 and (d)–(f) S2 NP shape in the (a) (d) L^2, (b) (e) P^2 and (c) (f) r^2 spaces.

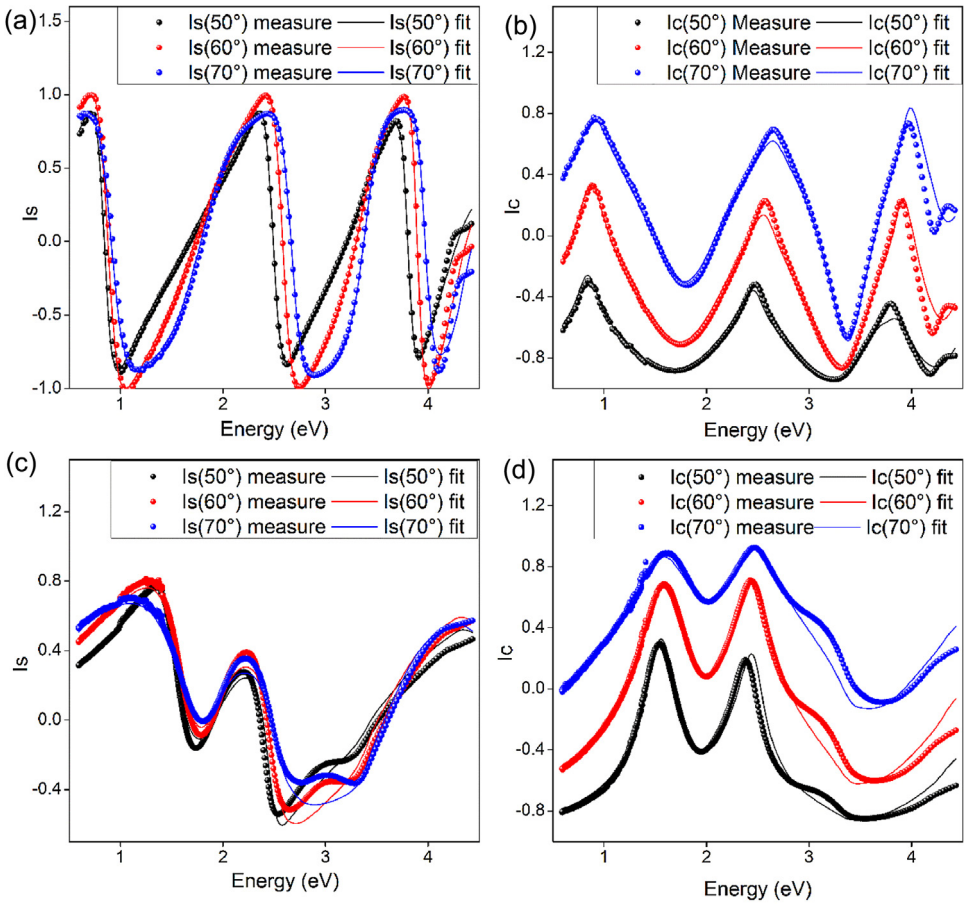

Fig. 7. Comparison between the measured and calculated ellipsometric spectra of (a) and (b) F1 and (c) and (d) F2.

be obtained between the volume fraction and the effective absorption coefficient [26]. In addition, the position of the plasmon band mainly depends on the mean value of depolarization factor while the width of the plasmon bands is mainly defined by the standard deviation of the distribution [26]. We also check that the initial input values have a negligible effect on the final results. As shown,

Please cite this article in press as: Y. Battie, et al., Determination of gold nanoparticle shape from absorption spectroscopy and ellipsometry, Appl. Surf. Sci. (2016), http://dx.doi.org/10.1016/j.apsusc.2016.12.167

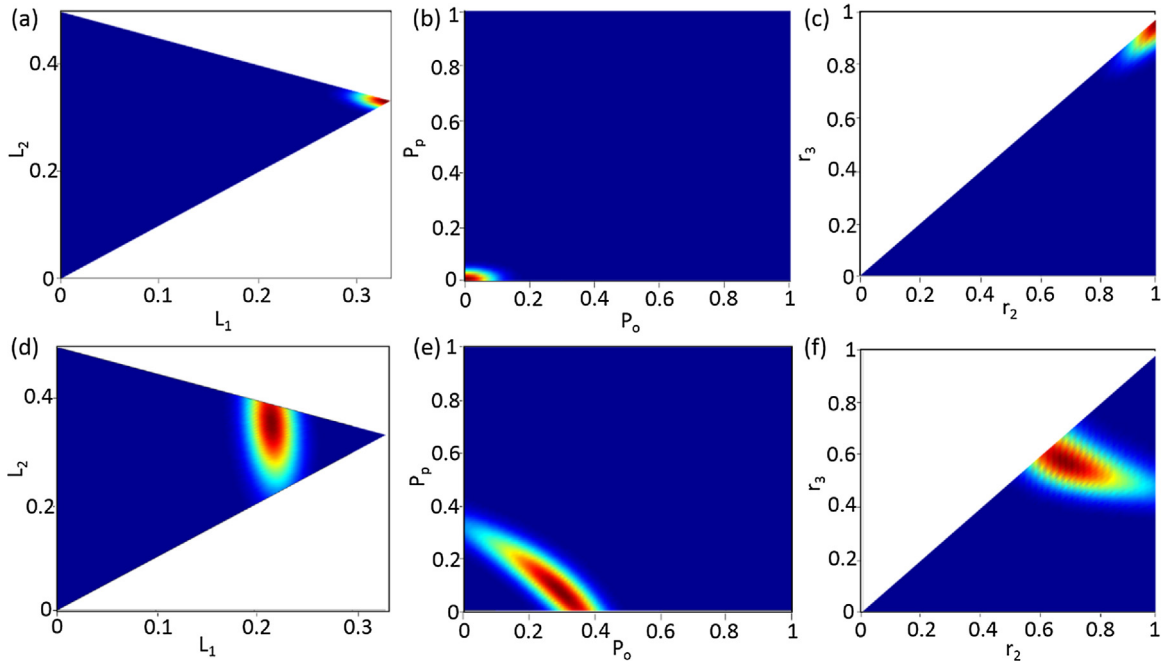

Fig. 8. Distributions of (a)–(c) F1 and (d)–(f) F2 NP shape in the (a) (d) L^2, (b) (e) P^2 and (c) (f) r^2 spaces.

Table 1
Sphericity, prolacity and oblacity parameters of S1, S2, F1 and F2 NPs.

	$\overline{P}_p$	$\overline{P}_o$	$\overline{P}_s$
S1	0	0	0
S2 (DS21)	0.08	0	0.08
S2 (DS22)	0	0.77	0. 77
F1	0.006	0.004	0.007
F2	0.07	0.3	0.31

in Fig. 5, a good agreement is found between the measured and the calculated spectra. The root mean square errors between the measured and calculated data are smaller than 0.08. In addition, the volume fraction of S1 NPs is estimated at 2.1×10^{-4}% confirming that the NPs are sufficiently diluted to neglect their mutual interaction.

The distributions of NP shape in the L^2, P^2 and r^2 spaces deduced from the absorption spectra analysis are reported in Fig. 6. In agreement with TEM (Figs. 2 and 4), the S1 distribution is centered on the locus of spherical NPs (Fig. 6a–c). Indeed, as summarized in Table 1, the sphericity parameter is close to zero. In addition, the distribution of aspect ratio in the r^2 space (Fig. 6c) matches the distribution obtained from TEM (Fig. 4a). Indeed, the aspect ratio of NP vary from 0.8 to 1 because a large number of S1 NPs are facetted and are not perfectly spherical. On the contrary, S2 distribution is the combination of two distributions ($DS2_1$ and $DS2_2$) (Fig. 6d–f). The volume fractions of NP associated to $DS2_1$ and $DS2_2$ are 2.5×10^{-4}% and 5.4×10^{-5}%, respectively. To make easier the interpretation, the oblacity, prolacity and sphericity parameters are calculated for each distribution (Table 1). The sphericity parameter of $DS2_1$ is estimated at 0.08 while the prolacity and the sphericity parameters of $DS2_2$ are 0 and 0.77, respectively. Indeed, S2 contains a mixture of nearly spherical NPs and nanorods assimilated to prolate NPs. The aspect ratio distribution in the r^2 space (Fig. 6f) is close to the one measured from TEM (Fig. 4b). However, only one aspect ratio per NPs can be measured from TEM because TEM provides a two dimensional projection of NPs. In addition, the NPs volume fraction cannot be determined by TEM. The volume of the colloidal solution probed by the light beam is 20 mm^3. By considering the volume fraction and the mean volume of NPs, we conclude that the distribution of NP shape is recorded over 10^{10}–10^{12} NPs.

The same procedure can be used to determine the NP shape distribution from ellipsometric measurements. Contrary to absorption spectroscopy, ellipsometry is sensitive to the real part and the imaginary part of dielectric function of materials. In addition, ellipsometric measurements in reflection mode enables the characterization of thin films deposited on opaque substrates. The ellipsometric spectra of F1 and F2 are shown in Fig. 7. To extract optical properties of nanocomposite layers from ellipsometric data, an optical model must be introduced. This model consists of a silicon substrate covered by a photoresist film which contains Au NPs. The optical properties of these films are described by an effective dielectric function calculated from SDEMT (7). The dielectric function of the matrix ε_m is set to the measured one on a photoresist film without gold precursor. In a classical approach, an intrinsic confinement effect occurs when the mean free path of conduction electrons is limited by the NP size. As we have shown previously [25], this effect becomes non-negligible for NP size smaller than 5 nm. In other words, by considering the NPs size deduced from TEM (Fig. 2c and d), the intrinsic confinement must be taken into account for F1 and F2. By assuming that the intrinsic confinement only affects free electrons, the dielectric function of Au NPs can be calculated from [1]:

$$(17)\ \varepsilon_{np}(l) = \varepsilon_{bulk} - \frac{\omega_p^2}{\omega(\omega+i\Gamma_0)} + \frac{\omega_p^2}{\omega\left(\omega+i\left(\Gamma_0+A\frac{v_f}{l}\right)\right)},$$

where ω is the photon energy and A a constant. ε_{bulk} is the bulk dielectric function of Au [32]. $\omega_p = 8.64$ eV, $\Gamma_0 = 0.097$ eV and $v_f = 1.4^{*}10^6$ m/s are the bulk plasma energy, the bulk electron damping and the Fermi velocity of free electrons, respectively [25]. l is the mean value of NP size. The value of the constant A depends on the NP shape [31], the scattering scheme [1,34], and the chemical environment of NPs [35–37]. As reported previously, confinement effect induced a broadening of the plasmon band and a decrease of its amplitude [1,25]. In addition, this effect induces a decrease of the absorption close to the interband transition threshold. The Abeles formalism [38] is used to calculate the ellipsometric parameters (Is, Ic). 8 free parameters are fitted by using the Levenberg-Marquardt algorithm: f, $\bar{L}_1$, $\bar{L}_2$, σ_1, σ_2, σ_3, A/l, and the film thickness. Since A and l are strongly cor-

Please cite this article in press as: Y. Battie, et al., Determination of gold nanoparticle shape from absorption spectroscopy and ellipsometry, Appl. Surf. Sci. (2016), http://dx.doi.org/10.1016/j.apsusc.2016.12.167

related, they cannot be fitted independently. Indeed, only the ratio A/l can be determined from ellipsometric measurements [39]. The parameters f, $\bar{L}_1$, $\bar{L}_2$, σ_1, σ_2 and σ_3 are fitted simultaneously. More details on the fitting procedure and the A/l values obtained from ellipsometry for F1 and F2 are given in reference [39].

As shown in Fig. 7, a good agreement is obtained between the experimental ellipsometric spectra and the calculated ones. The root mean square error between the simulated and the experimental data is smaller than 0.06 for both films. Moreover, the correlation matrix (not shown) suggests that all free parameters are independent. The volume fractions of NPs are estimated at $0.7\% \pm 0.05\%$ and $11\% \pm 0.1\%$ for F1 and F2, respectively. These values are close to the nominal ones, and are small enough to neglect the NP interaction, confirming the correctness of our model. By considering the film thickness and the volume fraction of NPs, the ellipsometric beam probes approximately 10^{11} NPs.

The NP shape distributions in the L^2, P^2 and r^2 spaces are reported in Fig. 8. In accordance with TEM (Fig. 4c and d), F1 has a narrow NP shape distribution centered on the locus of spherical NPs. Indeed, its sphericity parameter is 0.007. On the contrary, the NP shape distribution of F2 is more complex and broader than the NP shape distribution of F1. The low prolacity value supports that the majority of NPs in F2 are elongated along one direction. TEM measurements (Fig. 4d) reveal that the apparent aspect ratio of nanoparticles is in the 0.4–1 range. However, 30% of NPs have an aspect ratio close to 1 (Fig. 4d). TEM gives a two dimensional projection of NPs so, only one aspect ratio per NP can be measured by TEM. As a consequence, the aspect ratio estimated by TEM can be overestimated because non-spherical elongated nanoparticles could appear as closely spherical NPs, depending on their orientation. This supports that optical spectroscopy can be used to supplement TEM for the characterization of NP shape distribution.

5. Conclusion

In summary, we have developed an effective medium theory (SDEMT) to calculate the complex dielectric function of randomly oriented ellipsoïdal NPs distributed in shape. Three spaces L^2, P^2 and r^2 were introduced with the sphericity, prolacity and oblacity estimators to analyze the NP shape distribution. The P^2 space is used to quantify the degree of oblacity, prolacity and sphericity of NPs, while the distribution in r^2 space gives the aspect ratio of NPs. SDEMT and these spaces are used to extract the NP shape distribution and the volume fraction of Au nanoparticles in colloidal solutions and in photoresist films from their absorption and ellipsometric spectra, respectively. These distributions are close to the ones obtained from TEM. Contrary to TEM measurements, the NP shape distribution is obtained from a large number of NPs estimated at 10^{10}–10^{12} NPs. In addition, TEM only give the apparent aspect ratio of NPs while the method proposed here leads to the determination of the two aspects ratio of ellipsoidal NPs. Thus, we demonstrate that optical spectroscopy coupled with SDEMT, is an relevent alternative tool to TEM.

References

[1] U. Kreibig, M. Vollmer, Optical Properties of Metal Clusters, Springer, Berlin, 1995.
[2] D. Derkacs, S.H. Lim, P. Matheu, W. Mar, E.T. Yu, Improved performance of amorphous silicon solar cells via scattering from surface plasmon polaritons in nearby metallic nanoparticles, Appl. Phys. Lett. 89 (2006) 93103.
[3] H.A. Atwater, A. Polman, Plasmonics for improved photovoltaic devices, Nat. Mater. 9 (2010) 205–213.
[4] P.M. Aneesh, C.R. Kumar, P.R. Varma, K. Vivek, M.A. Namboothiry, Enhancement in photovoltaic properties of plasmonic nanostructures incorporated organic solar cells processed in air using P3HT: PCBM as a model active layer, Org. Photonics Photovolt. 3 (2015) 64–70.
[5] P. Reineck, D. Brick, P. Mulvaney, U. Bach, Plasmonic hot electron solar cells: the effect of nanoparticle size on quantum efficiency, J. Phys. Chem. Lett. 7 (2016) 4137–4141.
[6] A.D. McFarland, R.P. Van Duyne, Single silver nanoparticles as real-time optical sensors with zeptomole sensitivity, Nano Lett. 3 (2003) 1057–1062.
[7] O. Peña, L. Rodriguez-Fernandez, V. Rodriguez-Iglesias, G. Kellermann, A. Crespo-Sosa, J.C. Cheang-Wong, H.G. Silva-Pereyra, J. Arenas-Alatorre, A. Oliver, Determination of the size distribution of metallic nanoparticles by optical extinction spectroscopy, Appl. Opt. 48 (2009) 566–572.
[8] V. Rodriguez-Iglesias, O. Peña-Rodriguez, H.G. Siva-Pereyra, L. Rodriguez-Fernandez, G. Kellermann, J.C. Cheang-Wong, A. Crespo-Sosa, A. Oliver, Elongated gold nanoparticles obtained by ion implantation in silica: characterization and T-matrix simulations, J. Phys. Chem. C 114 (2010) 745–751.
[9] C.R. Henry, Morphology of supported nanoparticles, Prog. Surf. Sci. 80 (2005) 92–116.
[10] F. Bouquard, A.S. Loir, C. Donnet, F. Garrelie, In situ diagnostic of the size distribution of nanoparticles generated by ultrashort pulsed laser ablation in vacuum, Appl. Phys. Lett. 104 (2014) 104101.
[11] M. Quinten, Optical Properties of Nanoparticles System: Mie and Beyond, Wiley-VCH, 2011.
[12] S. Eustis, M.A. El-Sayed, Determination of the aspect ratio statistical distribution of gold nanorods in solution from a theoretical fit of the observed inhomogeneously broadened longitudinal plasmon resonance absorption spectrum, J. Appl. Phys. 100 (2006) 044324.
[13] K. Slyusarenko, B. Abécassis, P. Davidson, D. Constantin, Morphology of gold nanoparticles determined by full-curve fitting of the light absorption spectrum. Comparison with X-ray scattering and electron microscopy data, Nanoscale 6 (2014) 13527–13534.
[14] Y. Battie, N. Destouches, F. Chassagneux, D. Jamon, L. Bois, N. Moncoffre, N. Toulhoat, Optical properties of silver nanoparticles thermally grown in a mesostructured hybrid silica film, Opt. Mater. Express. 1 (2011) 1019–1033.
[15] T.W.H. Oates, Real time spectroscopic ellipsometry of nanoparticle growth, Appl. Phys. Lett. 88 (2006) 213115.
[16] T.W.H. Oates, M. Ranjan, S. Facsko, H. Arwin, Highly anisotropic effective dielectric function of silver nanoparticle arrays, Opt. Express. 19 (2011) 2014–2028.
[17] H. Wormeester, E.S. Kooij, A. Mewe, S. Rekveld, B. Poelsema, Ellipsometric characterisation of heterogeneous 2D layers, Thin Solid Films 455–456 (2004) 323–334.
[18] B.T. Draine, P.J. Flatau, Discrete-dipole approximation for scattering calculations, J. Opt. Soc. Am. A 11 (1994) 1491–1499.
[19] U. Hohenester, J. Krenn, Surface plasmon resonances of single and coupled metallic nanoparticles: a boundary integral method approach, Phys. Rev. B 72 (2005) 195429.
[20] J. Toudert, L. Simonot, S. Camelio, D. Babonneau, Advanced optical effective medium modeling for a single layer of polydisperse ellipsoidal nanoparticles embedded in a homogeneous dielectric medium: surface plasmon resonances, Phys. Rev. B. 86 (2012) 045415.
[21] C.F. Bohren, D.R. Huffman, Absorption and scattering by a sphere, in: Absorption and Scattering of Light by Small Particles, Wiley, Germany, 1998.
[22] A.V. Goncharenko, A.O. Pinchuk, Broadband epsilon-near-zero composites made of metal nanospheroids, Opt. Mater. Express. 4 (2014) 1276–1286.
[23] Y. Battie, A. En Naciri, W. Chamorro, D. Horwat, Generalized effective medium theory to extract the optical properties of two-dimensional nonspherical metallic nanoparticle layers, J. Phys. Chem. C 118 (2014) 4899.
[24] Y. Battie, A. Resano-Garcia, A. En Naciri, S. Akil, N. Chaoui, Determination of morphological characteristics of metallic nanoparticles based on modified Maxwell-Garnett fitting of optical responses, Appl. Phys. Lett. 107 (2015) 143104.
[25] Y. Battie, A. Resano-Garcia, N. Chaoui, Y. Zhang, A. En Naciri, Extended Maxwell-Garnett-Mie formulation applied to size dispersion of metallic nanoparticles embedded in host liquid matrix, J. Chem. Phys. 140 (2014) 044705.
[26] A. Resano-Garcia, Y. Battie, A. En Naciri, S. Akil, N. Chaoui, Experimental and theoretical determination of the plasmonic responses and shape distribution of colloidal metallic nanoparticles, J. Chem. Phys. 142 (2015) 134108.
[27] T. Yamaguchi, S. Yoshida, A. Kinbara, Optical effect of the substrate on the anomalous absorption of aggregated silver films, Thin Solid Films 21 (1974) 173–187.
[28] D. Bedeaux, J. Vlieger, Optical Properties of Surfaces, John Wiley & Sons, New York, 1983.
[29] R. Lazzari, I. Simonsen, GranFilm: a software for calculating thin-layer dielectric properties and Fresnel coefficicents, Thin Solid Films 419 (2002) 124–136.
[30] B. Nikoobakht, M.A. El-Sayed, Preparation and growth mechanism of gold nanorods (NRs) using seed-mediated growth method, Chem. Mater. 15 (2003) 1957–1962.
[31] J. Marques-Hueso, R. Abargues, J.L. Valdés, J.P. Martínez-Pastor, Ag and Au/DNQ-novolac nanocomposites patternable by ultraviolet lithography: a fast route to plasmonic sensor microfabrication, J. Mater. Chem. 20 (2010) 7436–7443.
[32] E.D. Palik, Handbook of Optical Constants of Solids, Academic press handbook series, New York, 1985.
[33] K.A. Levenberg, Method for the solution of certain problems in least squares, Q. Appl. Math. 2 (1944) 164–168.

Please cite this article in press as: Y. Battie, et al., Determination of gold nanoparticle shape from absorption spectroscopy and ellipsometry, Appl. Surf. Sci. (2016), http://dx.doi.org/10.1016/j.apsusc.2016.12.167

[34] E.A. Coronado, G.C. Schatz, Surface plasmon broadening for arbitrary shape nanoparticles: a geometrical probability approach, J. Chem. Phys. 119 (2003) 3926–3934.
[35] K.P. Charlé, F. Frank, W. Schulze, The optical properties of silver microcrystallites in dependance on size and the influence of the matrix environment, Ber. Bunsenges. Phys. Chem. 88 (1984) 350.
[36] H. Hövel, S. Fritz, A. Hilger, U. Kreibig, M. Vollmer, Width of cluster plasmon resonances: bulk dielectric functions and chemical interface damping, Phys. Rev. B 48 (1993) 18178.
[37] U. Kreibig, Interface-induced dephasing of Mie plasmon polaritons, Appl. Phys. B 93 (2008) 79–89.
[38] R.M.A. Azzam, N.M. Bashara, Ellipsometry and Polarized Light, North-Holland Publishing Company, Amsterdam, 1977.
[39] Y. Battie, I. Izquierdo-Lorenzo, A. Resano-Garcia, A. En Naciri, S. Akil, P.M. Adam, S. Jradi, How to determine the morphology of plasmonic nanocrystals without transmission electron microscopy? J. Nanopart. Res. 18 (2016) 217.

Please cite this article in press as: Y. Battie, et al., Determination of gold nanoparticle shape from absorption spectroscopy and ellipsometry, Appl. Surf. Sci. (2016), http://dx.doi.org/10.1016/j.apsusc.2016.12.167